Evidence for Kinetically Limited Thickness Dependent Phase Separation in Organic Thin Film Blends

R. Banerjee,* J. Novák, C. Frank, C. Lorch, A. Hinderhofer, A. Gerlach, and F. Schreiber

Institut für Angewandte Physik, Universität Tübingen, Auf der Morgenstelle 10, 72076 Tübingen, Germany

(Received 8 February 2013; published 2 May 2013)

We present depth-resolved grazing incidence x-ray diffraction, grazing incidence small angle scattering and x-ray reflectivity studies on the structure of mixed C_{60} and diindinoperylene (DIP) films as a function of the mixing ratio. We observe enhanced out-of-plane order and smoothing of the mixed films compared to pure films upon coevaporation of DIP:C_{60} thin films (in different mixing ratio) which otherwise phase separate. The mixing ratio of molecules can be tuned to alter the in-plane crystallite size as well as the interisland distances of the mixing molecules. Real-time *in situ* grazing incidence x-ray diffraction measurements show the kinetics and thickness dependence of phase separation, which appears to proceed only after a certain thickness. The crystallite grain size of the individual phase separated components is significantly larger at the top of the film than at the bottom with implications for the understanding of devices.

DOI: 10.1103/PhysRevLett.110.185506 PACS numbers: 61.05.cf, 64.75.St, 81.05.Fb

Organic molecular semiconductors (OSCs) have attracted substantial research interest in recent years, in an effort to complement inorganic semiconductors, due to their attractive optical and structural properties. Several device applications, such as diodes, field-effect transistors up to all-organic integrated circuits, photodiodes, organic photovoltaics (OPV), and organic light emitting diodes have been demonstrated by OSCs based on polymers or small molecules such as C_{60}, acenes, perylene-derivatives, and phthalocyanines [1–7]. Since the structure and morphology have a strong influence on the performance, their control is mandatory, but the mechanisms of structure formation of OSCs and their mixtures (and indeed molecular materials in general) are not completely understood on a fundamental level [8–12].

One principal strategy in OPV employs the mixing of donor (*D*) and acceptor (*A*) molecules (bulk heterojunction) [13–15]. The resulting efficiency crucially depends on the interplay of the diffusion lengths of the excitons generated by the absorption of light and the structural length scales of the *D*:*A* mixture, such as the typical width of the *D* and *A* domains [15]. Controlling these structural length scales in *D*:*A* mixtures, which are potentially phase separating, is thus a key point in this field. In addition to the relevance for applications, this is also a challenge for the fundamental understanding of the structural evolution of mixtures. Some comparisons can be made to the rich area of binary alloys (i.e., mixtures of elementary systems) [16] and to organic bulk crystals [17]. In the latter field, due to the different ratio of the range of interactions to the size of the objects (molecules) as well as their inherent anisotropy in shape, additional parameters have to be considered, which can lead to an even broader range of scenarios [8,18]. An important further challenge also comes from the fact that applications of OSCs are typically based on thin films, so that issues related to their interfaces and kinetically controlled growth enter the scenario.

The main focus of the present study is the real-time and *in situ* observation of growth as well as post-growth structural characterization of two prototypical OSCs, diindinoperylene (DIP) and C_{60} [inset of Fig. 1(a)], coevaporated in different mixing ratios. DIP and C_{60} are relevant for OPV as a model *D*:*A* pair [19]. Grazing incidence diffraction (GID) was performed as a function of time during growth and also as a function of probing depth post growth, to observe the evolution of the in-plane Bragg peaks. X-ray reflectivity (XRR) and grazing incidence small angle x-ray scattering (GISAXS) measurements were performed for post-growth analysis of the out-of-plane structure and in-plane domain size of the mixed films, respectively.

In this Letter, we show that for coevaporated DIP:C_{60} with phase-separating tendency as used in OPV, the domain size is thickness (or growth time) dependent and thus kinetically limited. The coherent crystallite grain size as well as the interdomain distances of the mixing molecules, for a given thickness, can be tailored by tuning the mixing ratio of molecules. At the same time, we observe enhanced out-of-plane order and smoothing of the mixed films compared to pure films upon coevaporation of these mixed films in different mixing ratios. Our results provide fundamentally new insight into the basic understanding of the phase separation kinetics of these systems by demonstrating the intercorrelation between the lateral and the vertical length scales (or time) with substantial implications for the theoretical understanding of OPV.

Sublimation grade DIP and C_{60} were obtained from Institut für PAH Forschung Greifenberg, Germany, with 99.9% purity, and Creaphys with 99.9% purity, respectively. Films containing DIP and C_{60} with varying mixing ratio were coevaporated on Si wafers covered with a native

 © 2013 American Physical Society

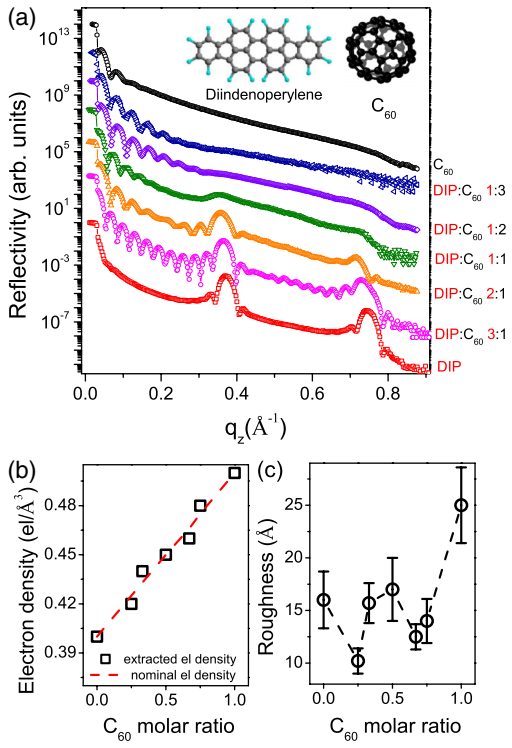

FIG. 1 (color online). (a) XRR profiles for the pure and the mixed films with various mixing ratios. The data have been scaled for clarity. The inset shows the molecular structure of DIP and C_{60}. (b) The average electron density derived from the fits of the XRR profiles. The dashed line shows the nominal electron density. (c) The top surface roughness and error bars derived from the XRR fits of the various films.

oxide layer (~ 9 Å) at a base pressure $< 5 \times 10^{-9}$ mbar. The growth rate monitored by XRR and a quartz crystal microbalance was ~ 0.4 nm/min. Apart from the pure films of DIP and C_{60}, five different molar mixing ratios of DIP:C_{60} (3:1, 2:1, 1:1, 1:2, 1:3) were investigated. The error in the stoichiometry of the mixtures is 10% determined by the error in the readout of the quartz-crystal microbalance. All films for *in situ* measurements were deposited up to a thickness of ~ 20 nm at a substrate temperature of 25 °C. Scattering measurements (viz. XRR, time and depth-resolved GID and GISAXS) were performed at the X04SA beam line of the Swiss Light Source at a wavelength of 0.99987 Å, in a custom-built portable organic molecular beam deposition chamber [20], using a Pilatus II detector.

XRR is used for the extraction of the electron density profile along the direction perpendicular to the sample surface and provides structural parameters like thickness and surface and interface roughness of thin films. The XRR profiles show distinct thickness oscillations for all the films and out-of-plane Bragg peaks for some of them [Fig. 1(a)]. It is evident from the XRR measurements that when DIP dominates the mixture, extremely smooth films are produced. The higher the ratio of DIP in the blend, the smoother is the film [see Fig. 1(a)]. For mixed thin films of DIP and C_{60}, the first Bragg peak was observed distinctly for DIP:C_{60} 3:1 ratio (henceforth called only 3:1) and 2:1. However, for 1:1, the Bragg peak is severely distorted and for further increase in the C_{60} molar concentration, i.e., for 1:2 and 1:3, the Bragg peak completely disappears. The C_{60} Bragg peak along the specular direction for pure as well as mixed films is not properly recognizable, because the C_{60} forms essentially untextured polycrystalline thin films with low structural order on bare Si substrates (in contrast to layered D/A heterostructures, showing a distinct $C_{60}(111)$ Bragg peak at ~ 0.75 Å^{-1}, if DIP serves as a template for C_{60} [21]).

The XRR data were fitted using the Parratt formalism [22,23] up to a value of the out-of-plane component of the momentum transfer vector (q_z) equal to 0.2 Å^{-1} to estimate the average electron density and the top layer roughness of the films. A single box model was used in order to limit the number of fitting parameters. The average electron density (ρ in el/Å^3) and the top surface roughness extracted from the XRR fits are plotted in Figs. 1(b) and 1(c). We observe that ρ increases linearly from the value of ρ_{DIP} to the value of $\rho_{C_{60}}$ which consolidates the fact that there is no preference for either species to dominate the growth. In view of the strong tendency to phase separate (see below), it is quite remarkable that DIP:C_{60} shows a smoothing effect upon mixing. Indeed, overall the roughness evolution appears to be nontrivial from a fundamental perspective, but its tunability via the mixing ratio may be exploited in applications demanding smooth interfaces.

GID probes reciprocal space at high in-plane scattering angles and provides information on the crystallinity of the samples. The post-growth GID measurements (Fig. 2) show the known in-plane Bragg reflections for C_{60} (rather

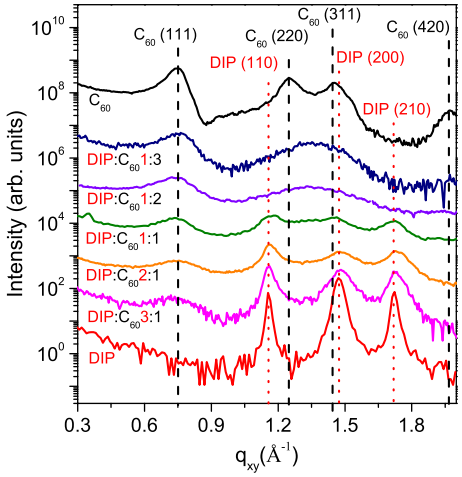

FIG. 2 (color online). GID plots of the pure films as well as the films with varying mixing ratio. All films were ~ 20 nm thick. The various peaks have been identified as either belonging to DIP thin film or C_{60} fcc thin film phases and no new or unidentified peaks were observed.

broad, as expected) and DIP [8,24]. The data show clear signs of phase separation since we can identify known peaks of pure DIP and C_{60} crystallites and no new or unidentified peaks even for mixed films with different ratios of mixing. Relative Bragg peak intensities from DIP and C_{60} correspond to the respective mixing ratios showing the expected predominance of the abundant species. The peak width for DIP is also seen to increase, signifying smaller grain sizes for smaller DIP content. For the mixing ratios 1:2 and 1:3, the DIP and C_{60} peaks cannot be discriminated and result in a broad hump around the in-plane component of the momentum transfer vector $q_{xy} = 1.3$ Å^{-1} where the peaks are expected. From the perspective of applications in OPV, another important consideration relates to the crystallite grain sizes which are either small (hence large number of grains) or big (hence fewer) for a fixed molar mixing ratio. For a given thickness, this is expected to be tunable by substrate temperature and rate of deposition. In the active region of a bulk heterojunction composed of a phase-separating D:A pair, smaller domains increase the surface area of exposure and hence the possibility for the excitons to reach the interface (where they eventually separate), but on the other hand decrease the charge mobility and hence the charge extraction. Optimizing the efficiency would thus be a tradeoff between the domain size (exciton exchange area) and the availability of percolation paths for charge transport.

GISAXS is sensitive to the morphology and preferential alignment of nanoscale objects at the surface. Additionally, it renders valuable information like the lateral correlations and sizes and shapes of nanostructures [23,25]. We observe distinct side peaks in the GISAXS measurements at different q_{xy}, depending on whether the thin film has a majority of DIP or C_{60} molecules [Figs. 3(a) and 3(b)]. The line profiles obtained from post-growth GISAXS measurements are shown in Fig. 3(a) and clearly exhibit differences in the in-plane characteristic length scales for the various mixed films. For mixtures with more DIP the peak maximum is closely spaced around the specular, i.e., large in-plane length scales in real space, but for mixtures with more C_{60}, the peaks are observed at larger q_{xy} suggesting smaller in-plane length scales. For the 1:1 mixture two distinct length scales are seen which correspond to the DIP and C_{60} phases. It is also observed that the characteristic length (or island distance) of one of the mixing molecules (say C_{60}) depends on the ratio of the other (DIP) [see Fig. 3(c)]. This can be exploited to prepare bulk heterojunctions with desired grain size as well as interdomain distance.

Having established the tendency for phase separation and the approximate in-plane correlations (island distances of the two respective components), a key question in film growth physics and for device architectures is whether this process is homogeneous or thickness dependent. To address this issue, we focus on the 1:1 mixing ratio which has been used in devices [19]. Real-time GID was

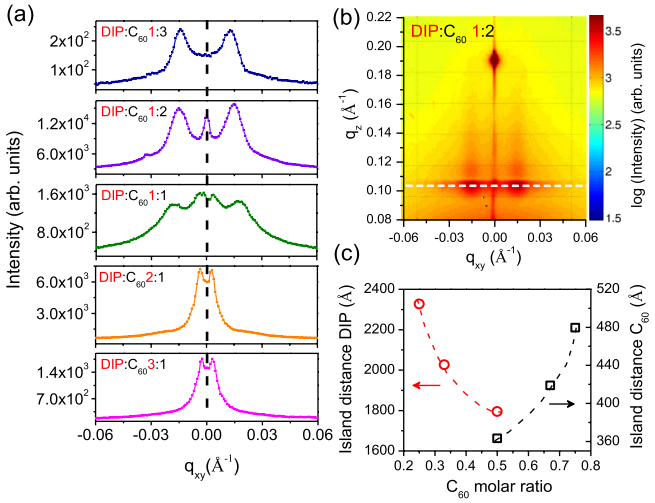

FIG. 3 (color online). (a) GISAXS line profiles of the DIP and C_{60} mixed films at final stages of growth. The position of the correlation peak clearly indicates that the C_{60} island distances are smaller in size than the DIP islands. For the 1:1 mixture, two distinct length scales are seen corresponding to C_{60} and DIP molecules. (b) Representative GISAXS data for 1:2 mixed film. The white dashed line shows the line scan from which characteristic length scales have been derived. (c) The characteristic length scales (island distances) for DIP and C_{60} as a function of the molar ratio. The dashed lines are guides to the eye.

performed to investigate the kinetics of phase separation during the growth process. The incident angle (θ_i) for GID measurements was 0.13° corresponding to a penetration depth of the entire film thickness. The real-time GID measurements (see Fig. 4) show that the GID peaks start to appear (i.e., crystallites of DIP and C_{60} start forming) only after a certain thickness and become more intense as the growth progresses. We speculate that there is a delayed onset of crystallization and phase separation until a certain thickness is reached. This is obviously kinetically determined for a nonequilibrium growth process. Also, it is intuitively plausible that the crystallization process is delayed for a statistical mixture with two different molecules than for the one with just the pristine molecule. Below this thickness, the molecules are probably still in a mixed, albeit noncrystalline phase, but as soon as this thickness is reached, they start to phase separate and further growth of the mixed film only increases the lateral grain size of the phase-separated molecular domains. A schematic of the proposed model of growth is shown in Fig. 4.

To corroborate our model further and to demonstrate that the thickness-dependent lateral crystallite sizes are not a transient effect but rather prevail, we performed post-growth *ex situ* depth-resolved GID additionally on two films in ambient conditions to ensure that there is no significant post-growth structural reorganization in the mixed films. GISAXS probes the top surface structures and even by varying θ_i the buried structures cannot be easily probed due to the weak scattering contrast between

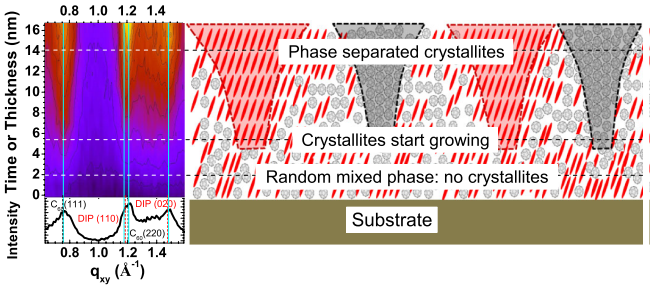

FIG. 4 (color online). (Left) Contour plot of real-time GID data measured during growth of 1:1 mixed film. Contour lines indicate levels with equal intensity. GID data from the final thickness have been plotted at the bottom. The blue lines indicate the peak maxima. (Right) Schematic reprsesentation of the model proposed for the kinetically driven phase separation during the growth of a coevaporated DIP and C_{60} thin film. The molecules phase-separate into domains of crystallites which grow laterally with increasing thickness of the film.

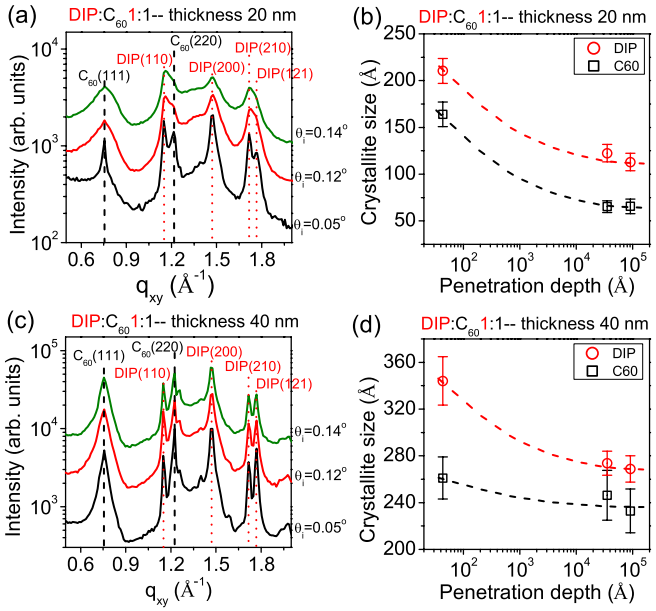

FIG. 5 (color online). (a) Depth-resolved GID measurements of a 20 nm mixed film with ratio 1:1. (b) The average crystallite size estimated from the GID peaks using the Scherrer formula for the 20 nm film. It is observed that the crystallites at the top surface are much larger than at the bottom. (c) Depth-resolved GID measurements of a thicker (40 nm) film. Here, clear separation of the GID peaks is seen suggesting larger crystal grains for both DIP and C_{60}. (d) The average crystal grain size for the 40 nm film is much larger than that for the 20 nm film and one observes the same trend of increased grain size at the top surface. The dashed lines are guides to the eye.

DIP and C_{60}. Depth-resolved GID, on the other hand, probes the variation of the ''coherent'' lateral crystallite size at different depths of the film. For the 20 nm and 40 nm 1:1 mixed films, we performed depth-resolved GID by changing θ_i and hence the penetration depth of the impinging x rays. Figure 5 shows that the peaks are better resolved at a very low penetration depth (50 Å corresponding to $\theta_i = 0.05°$), clearly indicating that the grain size at the top surface of the film is larger than near the bottom (film-substrate) interface for both films. The size of the crystallites estimated by the Scherrer formula is shown in Fig. 5 for DIP and C_{60} as a function of penetration depth. We already penetrate the entire film at $\theta_i = 0.12°$ so the estimated crystallite size does not change on further increments of θ_i to 0.14°. For the thicker film (40 nm) we observe that the peaks are even better resolved and sharper than in the 20 nm film for the different depths of penetration. We observe larger lateral grain size for both constituents with increasing film thickness from 20 nm to 40 nm (see Fig. 5). The growth model (Fig. 4) is thus also valid for the 40 nm film but with larger crystallite grains than in the 20 nm film.

In conclusion, using surface-sensitive scattering techniques we have consistently shown that the coevaporation of two prototypical small-molecule OSCs with a tendency for phase separation leads to a thickness and growth-time dependent domain size. We speculate that this is a rather general phenomenon in kinetically limited growth of phase separating systems, most likely not limited to OSCs. This means that the relationship between the structural length scales and those relevant for the functioning of a device, namely exciton diffusion and carrier transport, can be vastly different for the region near the top vs that near the bottom electrode and particular attention has to be paid to top-to-bottom asymmetry in mixed layers, as observed in our study. Qualitative agreement between real-time GID and post-growth depth-resolved GID is established, which is consistent with the growth model proposed. The characteristic length scales probed by GISAXS demonstrate clear dependence of island distances on the mixing ratio of molecules. The results have substantial implications for the fundamental understanding of the phase separation kinetics of these systems as well as the modeling of device architectures of *D*:*A* blends.

We acknowledge P. Willmott and S. Leake for experimental assistance at the SLS. We acknowledge financial support by the DFG, the Carl-Zeiss-Stiftung, and the EU.

*rupak.banerjee@uni-tuebingen.de

[1] W. Brütting and C. Adachi, *Physics of Organic Semiconductors* (Wiley-VCH, Weinheim, 2012), 2nd ed.
[2] W. R. Salaneck, K. Seki, A. Kahn, and J.-J. Pireaux, *Conjugated Polymer and Molecular Interfaces* (Marcel Dekker Inc., Basel, 2001).
[3] S. R. Forrest, Chem. Rev. **97**, 1793 (1997).
[4] C. Deibel and V. Dyakonov, Rep. Prog. Phys. **73**, 096401 (2010).
[5] G. Dennler, M. C. Scharber, and C. J. Brabec, Adv. Mater. **21**, 1323 (2009).

[6] P. Peumans, S. Uchida, and S. R. Forrest, Nature (London) **425**, 158 (2003).
[7] P. Peumans, A. Yakimov, and S. R. Forrest, J. Appl. Phys. **93**, 3693 (2003).
[8] A. Hinderhofer and F. Schreiber, ChemPhysChem **13**, 628 (2012).
[9] C. Schünemann, D. Wynands, L. Wilde, M. P. Hein, S. Pfützner, C. Elschner, K.-J. Eichhorn, K. Leo, and M. Riede, Phys. Rev. B **85**, 245314 (2012).
[10] H. J. Kim, J. W. Kim, H. H. Lee, B. Lee, and J.-J. Kim, Adv. Funct. Mater. **22**, 4244 (2012).
[11] A. C. Dürr, F. Schreiber, K. A. Ritley, V. Kruppa, J. Krug, H. Dosch, and B. Struth, Phys. Rev. Lett. **90**, 016104 (2003).
[12] S. Kowarik, A. Gerlach, S. Sellner, F. Schreiber, L. Cavalcanti, and O. Konovalov, Phys. Rev. Lett. **96**, 125504 (2006).
[13] C. W. Tang, Appl. Phys. Lett. **48**, 183 (1986).
[14] M. Zhang, H. Wang, H. Tian, Y. Geng, and C. W. Tang, Adv. Mater. **23**, 4960 (2011).
[15] A. Opitz, J. Wagner, W. Brütting, I. Salzmann, N. Koch, J. Manara, J. Pflaum, A. Hinderhofer, and F. Schreiber, IEEE J. Sel. Top. Quantum Electron. **16**, 1707 (2010).
[16] H. Dosch, *Critical Phenomena at Surfaces and Interfaces* (Springer-Verlag, Berlin, 1992).
[17] A. Kitaigorodsky, *Mixed Crystals* (Springer, Berlin, 1984).
[18] A. Aufderheide, K. Broch, J. Novák, A. Hinderhofer, R. Nervo, A. Gerlach, R. Banerjee, and F. Schreiber, Phys. Rev. Lett. **109**, 156102 (2012).
[19] J. Wagner, M. Gruber, A. Hinderhofer, A. Wilke, B. Bröker, J. Frisch, P. Amsalem, A. Vollmer, A. Opitz, N. Koch, F. Schreiber, and W. Brütting, Adv. Funct. Mater. **20**, 4295 (2010); M. Gruber *et al.*, Adv. Energy Mater. (in press).
[20] K. A. Ritley, B. Krause, F. Schreiber, and H. Dosch, Rev. Sci. Instrum. **72**, 1453 (2001).
[21] A. Hinderhofer, A. Gerlach, K. Broch, T. Hosokai, K. Yonezawa, K. Kato, S. Kera, N. Ueno, and F. Schreiber, J. Phys. Chem. C **117**, 1053 (2013).
[22] L. G. Parratt, Phys. Rev. **95**, 359 (1954).
[23] M. Tolan, *X-ray Scattering from Soft-Matter Thin Films* (Springer, Berlin, 1999); J. Daillant and A. Gibaud, *X-ray and Neutron Reflectivity: Principles and Applications* (Springer, Paris, 1999).
[24] M. A. Heinrich, J. Pflaum, A. K. Tripathi, W. Frey, M. L. Steigerwald, and T. Siegrist, J. Phys. Chem. C **111**, 18 878 (2007).
[25] R. Lazzari, J. Appl. Crystallogr. **35**, 406 (2002).